






The 3D OrbiSIMS—label-free metabolic imaging with subcellular lateral resolution and high mass-resolving power

Melissa K Passarelli¹, Alexander Pirkel², Rudolf Moellers², Dmitry Grinfeld³, Felix Kollmer², Rasmus Havelund¹ , Carla F Newman⁴, Peter S Marshall⁴, Henrik Arlinghaus² , Morgan R Alexander⁵ , Andy West⁴, Stevan Horning³, Ewald Niehuis² , Alexander Makarov³, Colin T Dollery⁴ & Ian S Gilmore¹ 

We report the development of a 3D OrbiSIMS instrument for label-free biomedical imaging. It combines the high spatial resolution of secondary ion mass spectrometry (SIMS; under 200 nm for inorganic species and under 2 μm for biomolecules) with the high mass-resolving power of an Orbitrap (>240,000 at m/z 200). This allows exogenous and endogenous metabolites to be visualized in 3D with subcellular resolution. We imaged the distribution of neurotransmitters—gamma-aminobutyric acid, dopamine and serotonin—with high spectroscopic confidence in the mouse hippocampus. We also putatively annotated and mapped the subcellular localization of 29 sulfoglycosphingolipids and 45 glycerophospholipids, and we confirmed lipid identities with tandem mass spectrometry. We demonstrated single-cell metabolomic profiling using rat alveolar macrophage cells incubated with different concentrations of the drug amiodarone, and we observed that the upregulation of phospholipid species and cholesterol is correlated with the accumulation of amiodarone.

Aberrant regulation of biomolecules can lead to devastating pathologies. Therefore, methods that detect and identify metabolites with subcellular spatial resolution would be valuable for studying diseases as well as to provide fundamental biological insights into metabolism heterogeneity at the single-cell scale. The metabolites expressed by a cell are indicative of its physiological state at a given time. The growing appreciation of the heterogeneous nature of metabolism motivates the need to measure and understand metabolite and phenotype variations at the single-cell level^{1–4}. In the pharmaceutical industry, there is a pressing need to improve drug efficacy and to reduce attrition (failure)⁵, especially during late-stage drug development. Metabolic imaging with subcellular lateral resolution would permit study of the effects of pharmaceuticals on cellular processes and identification of potential toxicological effects. A label-free method is needed

that can identify where drugs go to establish whether drug concentrations are sufficiently high in the right places to have a therapeutic effect, or if the medicine is concentrating within organelles and causing toxicity⁶.

As was recently highlighted, there are numerous analytical challenges associated with measuring the metabolome at the single-cell level². These include high-dynamic fluctuations, chemical diversity spanning a large dynamic range, the inability to amplify or tag metabolites, and the limited amount of material in a single cell. Single-cell measurements require a sensitive, label-free method with high chemical specificity and dynamic range. Mass spectrometry (MS) imaging offers label-free imaging capabilities and, for certain analytes, has subfemtomole sensitivity⁴.

The quest for subcellular-resolution metabolic imaging using MS has led to significant advances in instrumentation. Recent developments in high-resolution mass spectrometers—for example, the Orbitrap mass analyzer⁷, with a mass-resolving power in the range of 10^5 – 10^6 , a mass accuracy of <1 p.p.m. and tandem MS (MS/MS) capability, facilitates direct identification of metabolites from databases such as LIPID MAPS⁸. An elegant atmospheric pressure matrix assisted laser-desorption ionisation (AP-MALDI) MS source that combines an Orbitrap MS with a tightly focused laser beam was recently reported⁹; the authors demonstrated sampling regions as small as 1.44 μm in diameter and a lateral resolution for tissue classification of 2.9 μm . The highest reported MALDI MS spatial resolution was generated using a transmission geometry approach, which allowed imaging of tissue proteins with a laser spot diameter of 1 μm and a 2.5- μm step size¹⁰.

Secondary ion MS (SIMS) is an increasingly popular method in the life sciences^{11,12}, since it provides high spatial resolution using a focused ion beam as the probe and can image in 3D with ~5-nm-depth resolution^{13,14}. There have been significant developments to improve its application for biological studies, particularly to include MS/MS capability for identification of biomolecules. Such

¹National Physical Laboratory, NiCE-MSI, Teddington, Middlesex, UK. ²ION-TOF GmbH, Münster, Germany. ³Thermo Fisher Scientific, Bremen, Germany.

⁴GlaxoSmithKline, Stevenage, UK. ⁵School of Pharmacy, The University of Nottingham, Nottingham, UK. Correspondence should be addressed to I.S.G. (ian.gilmore@npl.co.uk).

developments include a quadrupole orthogonal time of flight (ToF) spectrometer¹⁵, the J105 (IONOPTIKA, UK) using a novel ToF-ToF design for continuous (nonpulsed) large cluster ion beams more suited to the detection of large biomolecules¹² than small cluster ion beams and the recent addition of a linear ToF to a TRIFT (Physical Electronics, Minnesota, USA) spectrometer that allows parallel MS/MS imaging¹⁶.

Fourier Transform mass spectrometers¹⁷ are the most accurate mass spectrometers for biomolecule identification, since they have the highest mass-resolving power and mass accuracy, and they are capable of high-resolution MS/MS. The first attempt to couple high spatial resolution SIMS with spectrometry with high mass-resolving power combined a liquid metal ion gun with a Bruker Daltonics 7.0 T APEX II (Bruker, Germany) Fourier Transform Ion Cyclotron Resonance (FT-ICR) MS¹⁸; the authors demonstrated the ability to acquire spectra from a 50 $\mu\text{m} \times 50 \mu\text{m}$ pixel with 30,000 mass-resolving power. Another group¹⁹ combined a C_{60} primary ion beam with a FT-ICR instrument and achieved a spatial resolution of $\sim 40 \mu\text{m}$ and 100,000 mass-resolving power when imaging cholesterol in a rat brain section. However, the signal-to-noise ratio, even for the abundant cholesterol molecule, was low despite the large pixel size and long pixel acquisition time of 15 s.

The principal practical limitation of FT-ICR MS is that, although this instrument has the necessary mass resolution and accuracy, it lacks the speed needed for capturing 3D or large 2D images; conversely, axial-ToF analyzers have the speed, but they lack the necessary accuracy to obtain chemical formulae. To overcome this dichotomy, we have developed the 3D OrbiSIMS, which uses a hybrid mass analyzer design. The 3D OrbiSIMS combines the strengths of high-speed ToF imaging with the high mass-resolving power, high mass accuracy and MS/MS capability of the Q Exactive

HF Orbitrap (Thermo Fisher Scientific, Germany)^{20,21}. To demonstrate the potential of the method, we examine the distribution of lipids and neurotransmitters in brain tissue and amiodarone-induced lysosomal dysfunction in macrophages.

RESULTS

The 3D OrbiSIMS instrument

We first describe the utility of the 3D OrbiSIMS from the perspective of a method for metabolic imaging and then provide technical instrument details for interested readers. A schematic of the instrument is given in **Figure 1**. The dual ion beam and dual analyzer configuration (**Fig. 1a**) provides ten operational modes for spectrometry, depth profiling, 2D and 3D imaging (**Fig. 1b**). For 2D imaging, a typical approach is to use the ToF analyzer with the bismuth liquid metal ion gun (Bi LMIG) to acquire a fast (~ 30 min) survey image and identify a region of interest (mode 6). Subsequently, an image can be acquired with the Orbitrap analyzer (mode 7), which gives high mass accuracy, high mass resolution and MS/MS capability. In this mode, the argon gas cluster ion beam (GCIB) is used, which creates mass spectra richer in intact biomolecules (e.g., lipids) and with significantly less fragmentation compared with a Bi LMIG primary ion beam²². Acquiring an image at the highest mass resolution with the Orbitrap is a slow process (a 256×256 pixel image with a mass resolving power of 240,000 at m/z 200 would take 9 h). Consequently, the ToF analyzer is needed.

SIMS enables high-resolution 3D molecular imaging and provides complementary information to other MSI methods such as AP-MALDI. In SIMS, a 3D image is created from a stack of 2D images acquired at different depths. The depth of the image is precisely controlled using an argon GCIB to gently sputter away

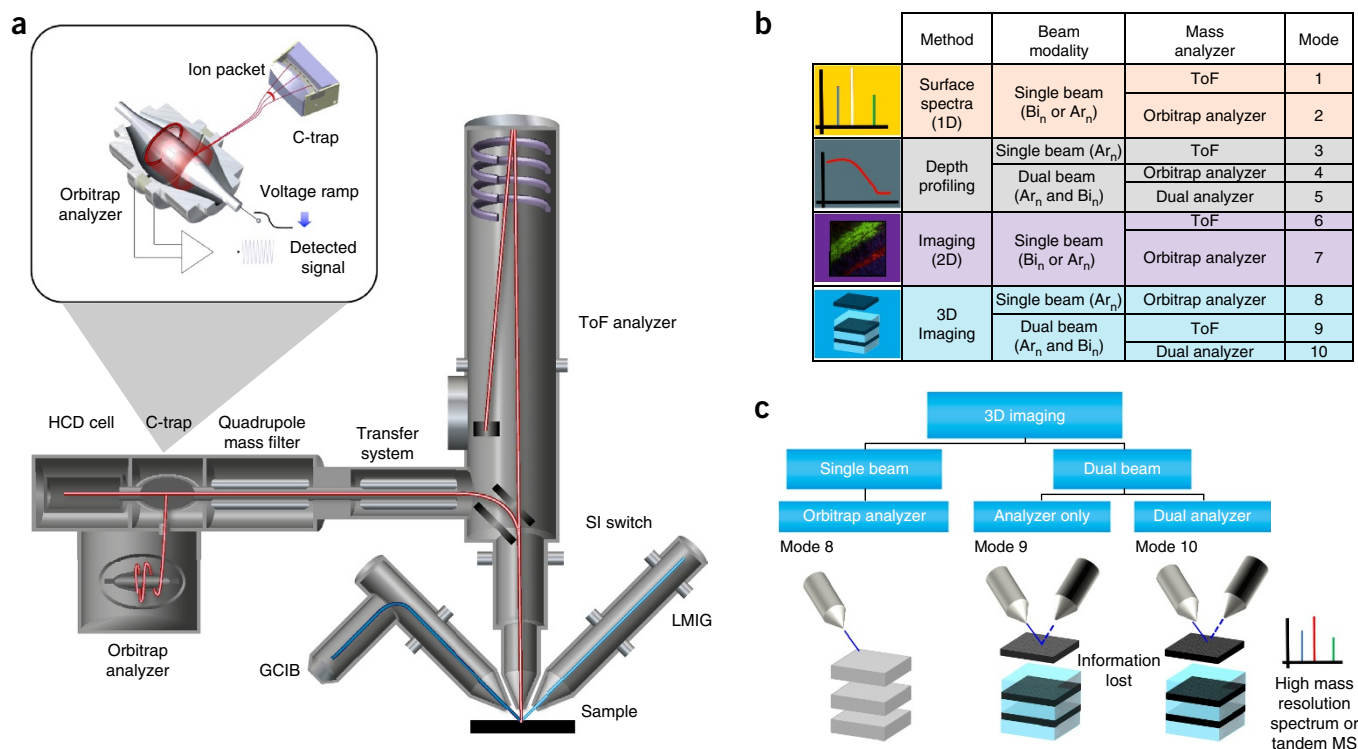


Figure 1 | The 3D OrbiSIMS spectrometer and modes of operation. **(a)** Schematic of the 3D OrbiSIMS. **(b)** Table of methodologies and data types achievable given the ion beam and spectrometer selections. **(c)** Hierarchy summary of 3D imaging modalities (modes 8–10).

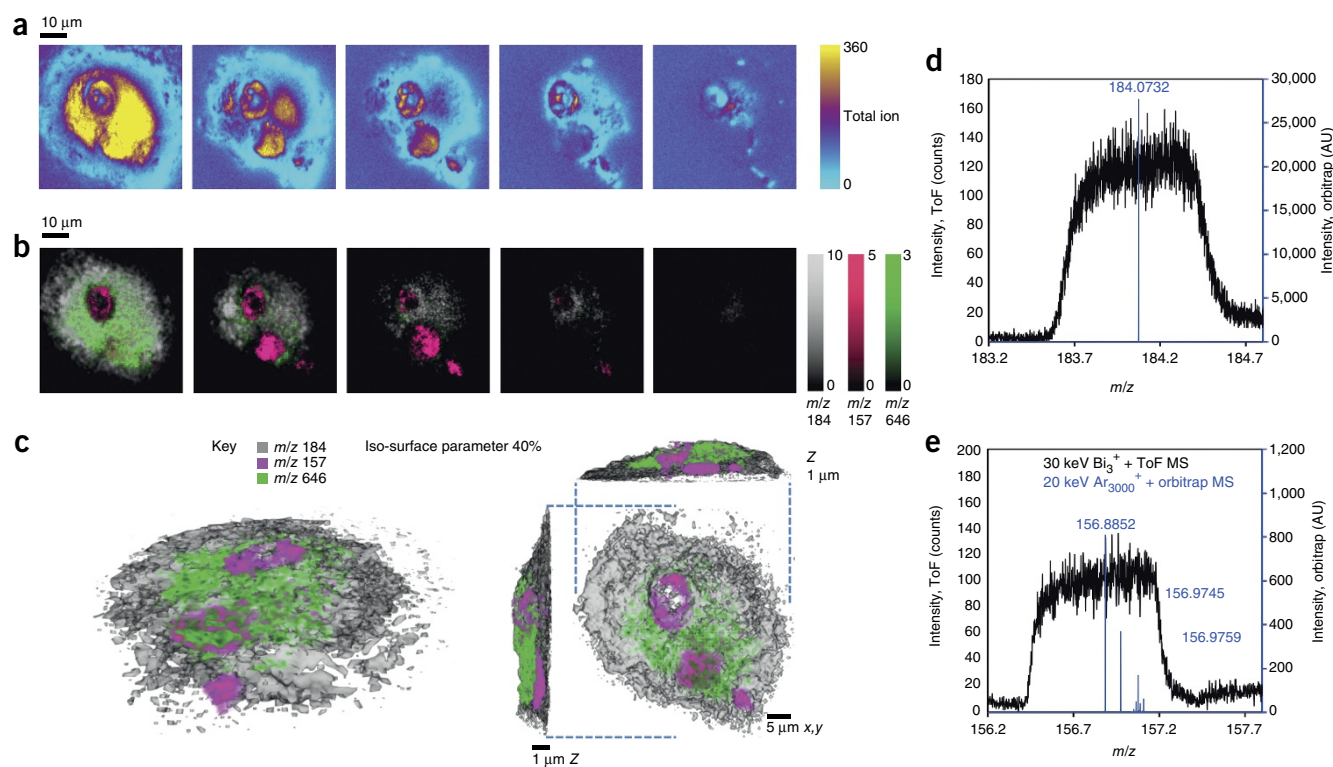


Figure 2 | 3D MS imaging using dual beam and dual spectrometer (mode 10) of single rat alveolar macrophage cell incubated in media with the drug amiodarone. (a) Sequence of 30 keV Bi_3^+ (~300-nm resolution) ToF-SIMS images of total ion counts at ~400-nm depths as the cell is sputtered away. (b) As in a, color overlay of phosphocholine marker (m/z 184, gray), nuclear marker (m/z 157, magenta) and amiodarone $[\text{M}+\text{H}]^+$ (m/z 646, green). (c) 3D rendering of the cell with phosphocholine marker, (m/z 184, gray, opacity 0.40), nuclear marker (m/z 157, magenta) and amiodarone $[\text{M}+\text{H}]^+$ (m/z 646, green). (d) High-mass-resolution spectrum from sputtered material using Orbitrap MS (blue) and low-mass-resolution spectra obtained during imaging with the ToF MS (black) for phosphocholine marker. (e) As in d for nuclear marker. Results presented are from a single measurement. AU, arbitrary units.

material. Our hybrid approach (mode 10) allows high-speed 3D imaging (Fig. 1c) using the Bi LMIG with ToF acquisition for high-spatial-resolution images and high-resolution mass spectra using the Orbitrap analyzer from the argon GCIB sputtering cycle between images.

An example of this new 3D imaging mode is demonstrated for a single alveolar macrophage cell incubated in media with the drug amiodarone at a concentration of 6.25 $\mu\text{g}/\text{mL}$ for 72 h (Fig. 2). A sequence of 2D ToF MS images at successive 400-nm depths (Fig. 2a,b) is reconstructed (see Online Methods) to produce a 3D image showing the distribution of amiodarone (Fig. 2c). The nucleus has an unusual shape, as was found in our previous ToF-SIMS imaging study²³. The high spatial resolution (~300 nm) ToF MS data with consequently poor mass resolution are complemented by the Orbitrap spectra (Fig. 2d,e), which allows cell membrane (m/z 184.0732, $\text{C}_5\text{H}_{15}\text{NO}_4\text{P}^+$) and nuclear marker ions (m/z 156.8852, K_2PO_4^+ ; m/z 156.9745, $\text{C}_2\text{H}_8\text{O}_2\text{P}_3^+$) to be putatively annotated. A weaker interference ion is also evident at m/z 156.9759 and is putatively annotated as $\text{C}_{10}\text{H}_9\text{N}_2^+$.

Instrument details

The 3D OrbiSIMS is based on the TOFSIMS 5 platform (ION-TOF GmbH, Germany), which we hybridize with a Q Exactive HF Orbitrap (Thermo Fisher Scientific, Germany) MS (Fig. 1a). The Orbitrap analyzer provides high mass accuracy (sub-p.p.m.), a high mass-resolving power (from 15,000 at m/z 200 with an acquisition rate >20 spectra up to 480,000 at m/z 200 with 1 spectrum),

high sensitivity and a high in-spectrum dynamic range (10^5 for ratio of total ion counts to noise). This is demonstrated by resolving the fine isotope structure of the mass spectrum of crystal violet (Supplementary Fig. 1 and Supplementary Table 1).

Both analyzers share the same secondary ion extraction optics (2,000 V potential) and consequently analyze the same point on the sample using either the 30 keV Bi LMIG or a microfocused 5–20 keV Ar_{3000}^+ GCIB with clusters in the range $1,000 < n < 10,000$ (see Online Methods). At the heart of the 3D OrbiSIMS is an electrostatic 90° deflector that selects either the ToF MS or, by 90° deflection, the Orbitrap MS. The deflector can be pulsed with a frequency of up to 30 kHz. With the Orbitrap selected, the secondary ions pass into the transfer system, where they are decelerated to kinetic energies of several tens of eV and are transferred via RF ion guides to the Q Exactive. To reduce the energy spread of the secondary ions, the transfer system comprises a multistage collisional damping cell. This replaces the standard ESI source and atmospheric pressure to vacuum interface of the Q Exactive HF. All other components remain unaffected, which allows for acquisition of either MS or MS/MS experiments with high mass resolution and mass accuracy for structural-based identification (Supplementary Fig. 2).

The microfocused GCIB, in combination with the Orbitrap MS, enables simultaneous high mass-resolving power and subcellular resolution. The resolution of the ion beam is measured (see Online Methods) by imaging an electroformed mesh grid from the ion-induced secondary electron image (Supplementary Figs. 3 and 4).

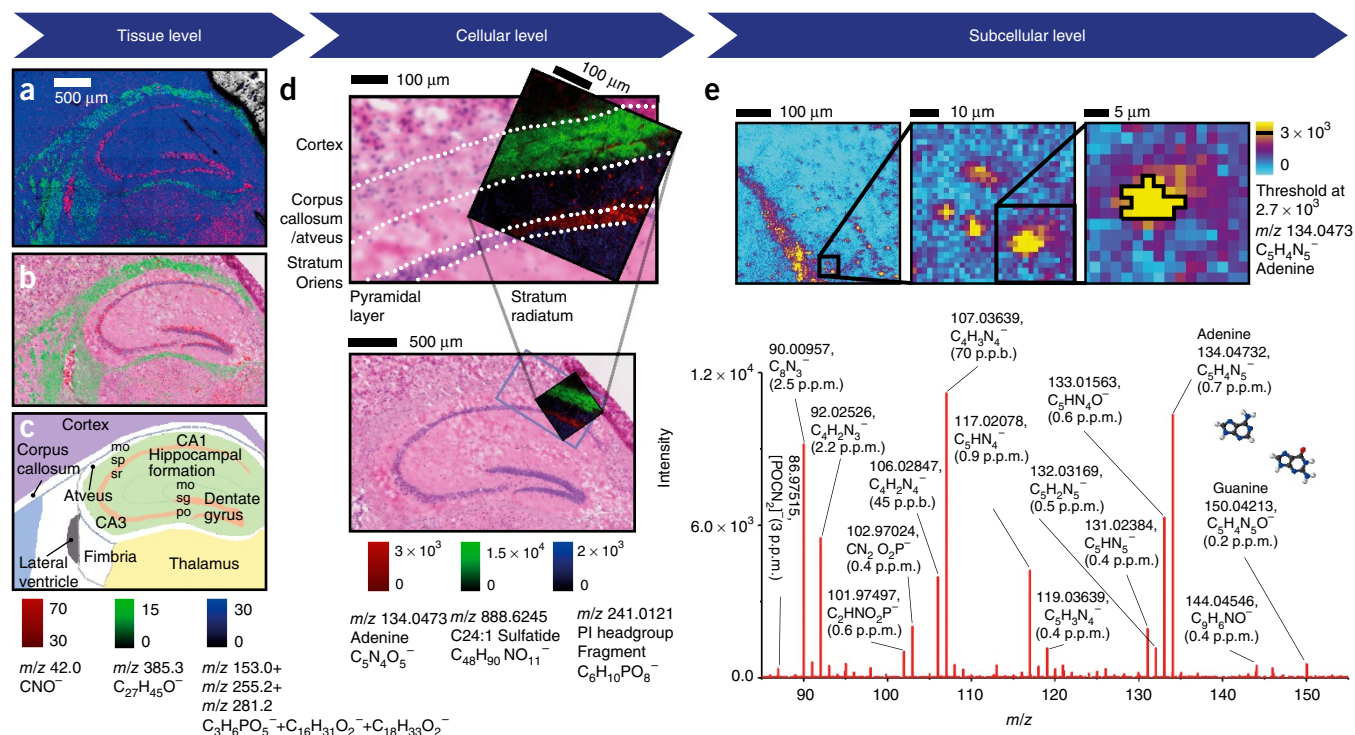


Figure 3 | 3D OrbiSIMS MS images of the hippocampal region of a coronal section of mouse brain at tissue scale, cellular scale and subcellular scale. (a) 30 keV Bi_3^+ (lateral resolution $\sim 2 \mu\text{m}$, pixel size $2 \mu\text{m}$) ToF MS image (mode 6) of the hippocampus region of a coronal mouse brain section, cholesterol (m/z 385.3, $\text{C}_{27}\text{H}_{45}\text{O}^-$, green), the small molecule (m/z 42.0, CNO^- , red) and glycerophospholipid fragments (the summed contribution of m/z 153.0 $\text{C}_3\text{H}_6\text{PO}_5^-$, m/z 255.2 $\text{C}_{16}\text{H}_{31}\text{O}_2^-$ and m/z 281.2 $\text{C}_{18}\text{H}_{33}\text{O}_2^-$, blue). (b) The distributions of cholesterol and CNO^- in the ion image are overlaid with the histological features in the adjacent H&E-stained brain section. (c) Schematic outlining the anatomical regions of the brain tissue. (d) 20 keV Ar_{3000} (lateral resolution $\sim 2 \mu\text{m}$, pixel size $1.95 \mu\text{m}$) Orbitrap MS image (mode 7) of the CA1 region, the phosphoinositol headgroup (m/z 241.0121, $\text{C}_6\text{H}_{10}\text{PO}_8^-$, blue), C24:1 Sulfatide m/z 888.6245, (3'-sulfo)Gal β -Cer(d18:1/24:1) ($\text{C}_{48}\text{H}_{90}\text{NO}_{11}^-$, green) and adenine (m/z 134.0473, $\text{C}_5\text{H}_4\text{N}_5^-$, red). Image is overlaid on the adjacent H&E-stained brain section for orientation. Boundaries between anatomical regions shown with white dashed lines. (e) Detail of d for adenine (m/z 134.0473, $\text{C}_5\text{H}_4\text{N}_5^-$) showing individual nuclei in the SO region with the background-subtracted mass spectrum of a single nuclei from a region of interest (black line), 15 pixels with intensity $> 2.7 \times 10^3$ threshold. Results presented are from a single measurement.

The secondary ion signal intensity is a further important parameter for the achievable practical resolution. In the absence of a suitable biologically relevant lateral-resolution reference device, we use two nuclei that exhibit clear chemical contrast to make x -axis and y -axis resolution measurements using the summed intensity of 8 nuclear markers (see Online Methods). The average resolution is determined to be $1.34 \mu\text{m} \pm 0.24 \mu\text{m}$ ($n = 5$) (Supplementary Fig. 5). It can be seen from Supplementary Figure 5 that the intensity of selected intact lipids is similar to the intensity of the selected nuclear markers, and therefore the spatial resolution will be similar. For inorganic materials, the Bi LMIG can be operated in a quasicontinuous mode in combination with the Orbitrap MS to give the highest simultaneous spatial resolution and mass-resolving power in relation to other MS imaging methods. We demonstrate (see Online Methods) a spatial resolution of $172 \text{ nm} \pm 61 \text{ nm}$ ($n = 95$) simultaneously with a mass-resolving power of 355 k for ZrO^+ (Supplementary Fig. 6) using Bi_3^{2+} .

The performance of 3D imaging and depth profiling is shown in more detail using a nanostructured reference material (Supplementary Fig. 7). The m/z 564 profiles show sharp peaks at the Irganox 3114 delta layers, where the signal rises over four orders of magnitude. A depth resolution (see Online Methods) of 11–13 nm is measured across all three modes. In modes 3

and 10, the secondary ions sputtered by the GCIB are analyzed with the Orbitrap MS. This is an advantage over conventional dual-beam depth profiling (mode 9), where the secondary ions sputtered by the GCIB, typically $>95\%$ of the sampled volume, are not used.

Molecular pathology

The structure of the hippocampus directs neural connectivity and influences cognitive abilities^{24–26}. We used the 3D OrbiSIMS to molecularly image the hippocampal region of a coronal section of mouse brain at tissue scale, cellular scale and subcellular scale (Fig. 3). The ion image (Fig. 3a) was aligned and overlaid onto the optical images of an adjacent H&E-stained tissue section (Fig. 3b) to provide complementary molecular pathology. The boundaries of anatomical regions of the brain (Fig. 3c) in the ion image were defined using the histological features in the H&E section and the Allen Brain Atlas²⁷.

At the tissue scale, a fast, large-field-of-view ToF-MS ion image (mode 6, mass-resolving power 5,000 at m/z 200, acquisition time 36 min) shows the distribution of cholesterol ($\text{C}_{27}\text{H}_{45}\text{O}$, $[\text{M}-\text{H}]^-$, m/z 385.3, green), the small molecular fragment CNO^- (m/z 42.0, red) and lipid fragments (the summed contribution of m/z 153.0 $\text{C}_3\text{H}_6\text{PO}_5^-$, m/z 255.2 $\text{C}_{16}\text{H}_{31}\text{O}_2^-$ and m/z 281.2 $\text{C}_{18}\text{H}_{33}\text{O}_2^-$, blue) (Fig. 3a).

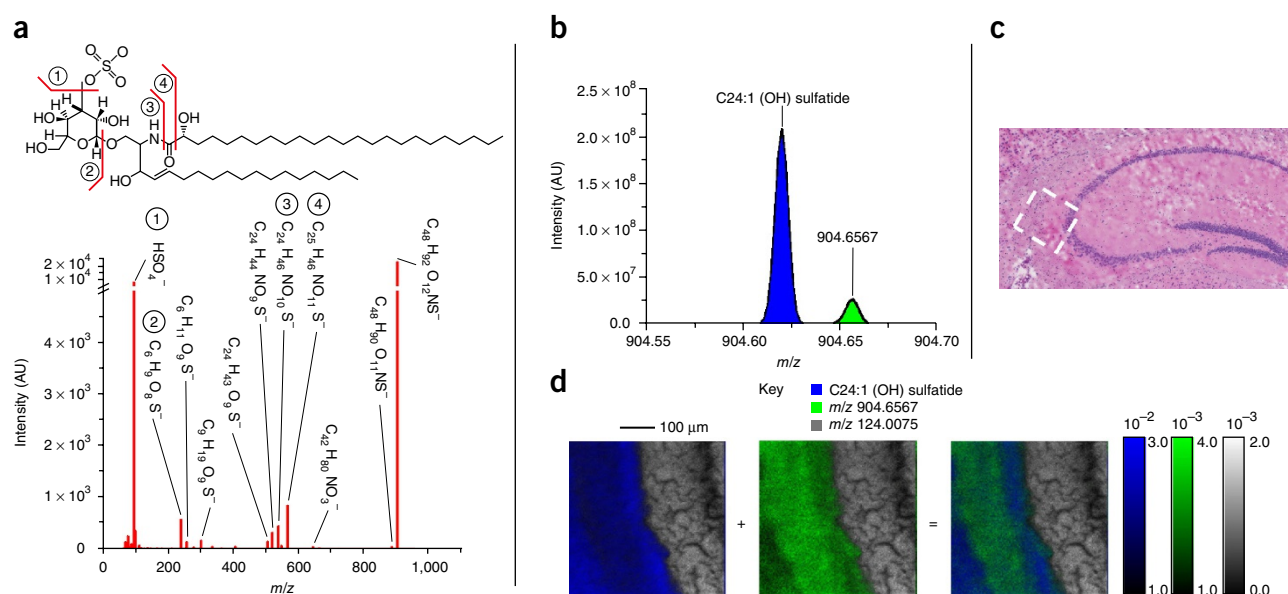


Figure 4 | Identification of lipids and mapping of their spatial distribution requires simultaneous high spatial resolution and high mass resolution as well as MS/MS. (a) 10-keV Ar₃₀₀₀ Orbitrap MS/MS (mode 2) of mass peak m/z 906.63 was used to identify the lipid species to be C24 (OH) sulfatide (3'-sulfo)Gal β -Cer(d18:1/24:0(2OH)). The chemical formula of each fragment peak assignment is provided. (b) 20 keV Ar₂₅₀₀ (lateral resolution $\sim 2 \mu\text{m}$, pixel size $1.95 \mu\text{m}$) Orbitrap mass spectrum (mode 7) showing a lipid molecule putatively annotated as C24:1 (OH) sulfatide (3'-sulfo)Gal-Cer(d18:1/24:1(2OH)), blue and a peak at m/z 904.65669. (c) Optical image of H&E-stained adjacent tissue section showing the region of analysis (white dotted line) and (d) Orbitrap MS images (parameters as a normalized to the total ion image of C24:1 (OH) sulfatide (blue), m/z 904.65669 (green) and m/z 124.0075 shown separately and as an overlay). Results presented are from a single measurement.

To demonstrate the improvement provided by the 3D OrbiSIMS, a section of the cornu ammonis 1 (CA1) region of the hippocampus was imaged with subcellular resolution ($\sim 2 \mu\text{m}$) and high mass-resolving power (240,000 at m/z 200, mode 7). The striated tissue layers in the hippocampus, stratum radiatum (SR), pyramidal layer (SP), stratum oriens (SO), corpus callosum (CC), and the cortex are chemically diverse. The cellular distribution of m/z 888.6245 putatively annotated as C24:1 sulfatide ((3'-sulfo)Gal β -Cer(d18:1/24:1)) in the CC layer is mapped in green (Fig. 3d). An advantage of argon GCIB is that there is little fragmentation of sulfatides, as is demonstrated for a reference sample of the same lipid (Supplementary Fig. 8). For phospholipids such as a phosphoethanolamine, however, there is significantly more fragmentation (Supplementary Fig. 9). The high density of cell bodies in the SP layer, stained purple-blue in the H&E image, correlated to the distribution of nuclear markers, adenine and guanine. Their summed contributions are shown in red in the ion image. This contrasts with the low density of neuronal cells in the SO and SR layers.

The instrument's mass-resolving power simultaneous with subcellular spatial resolution allows us to probe the chemical composition of a single nucleus. The nucleus of a single interneuron in the SO regions of the CA1 was selected, and the mass spectra for all the pixels in the region of interest (ROI) were summed (Fig. 3e). Purine-based nucleobases adenine and guanine, as well as phosphorylated species from the DNA, were detected²⁸. The high mass-resolving power at low molecular weight and high mass accuracy enabled putative annotation of the chemical formula of the signals.

These features also allowed the use of the LIPID MAPS database to putatively annotate 127 lipid species, including fatty acids, sterols, glycerophospholipids and sphingolipids (Supplementary Figs. 10 and 11; Supplementary Tables 2–8). The localizations

of 29 glycosphingolipid sulfatides were putatively annotated and mapped. Both hydroxylated and nonhydroxylated sulfatides with chain lengths ranging from 14 to 26 carbons with varying degrees of fatty acid saturation were identified. The presence and assignment of C24(OH) sulfatide ((3'-sulfo)Gal β -Cer(d18:1/24:0(2OH))) was confirmed with *in situ* MS/MS (Fig. 4a). Sulfatide lipids are abundant in the extracellular membrane of myelin and are responsible for the efficient conduction of electrical signals in the nervous system²⁹. These molecules play an important role in neurodegenerative diseases, such as Alzheimer's and Parkinson's disease, and the ability to detect and identify sulfatides and other lipids at subcellular lateral resolution will be beneficial to neuroscientists.

In many cases, the mass spectra, in the lipid mass range, showed multiple molecular ion signatures at the same nominal mass (Fig. 4b) from a region of the hippocampus (Fig. 4c). As shown in the ion image of the CA3 region (Fig. 4d), a peak at m/z 904.62012, putatively annotated as C24:1 (OH) sulfatide ((3'-sulfo)Gal-Cer(d18:1/24:1(2OH))) with a mass accuracy of 1.1 p.p.m. and a peak at m/z 904.65669 was chemically and spatially resolved. A minimum mass-resolving power of 25,000 is needed to resolve the two peaks (Supplementary Fig. 12).

Mapping molecules in neuronal communication

Neurons employ signaling molecules, or neurotransmitters, to communicate. These include glutamate, gamma-aminobutyric acid (GABA), dopamine, norepinephrine, epinephrine, histamine, serotonin and acetylcholine. The 3D OrbiSIMS enables mapping of multiple neurotransmitter distributions in neural tissue (Fig. 5a) in a single experiment. The putatively annotated neurotransmitters, GABA or isomer ($\text{C}_4\text{H}_8\text{NO}_2^-$ at m/z 102.0560), dopamine (Fig. 5b) ($\text{C}_8\text{H}_{10}\text{NO}_2^-$ at m/z 152.0718) and

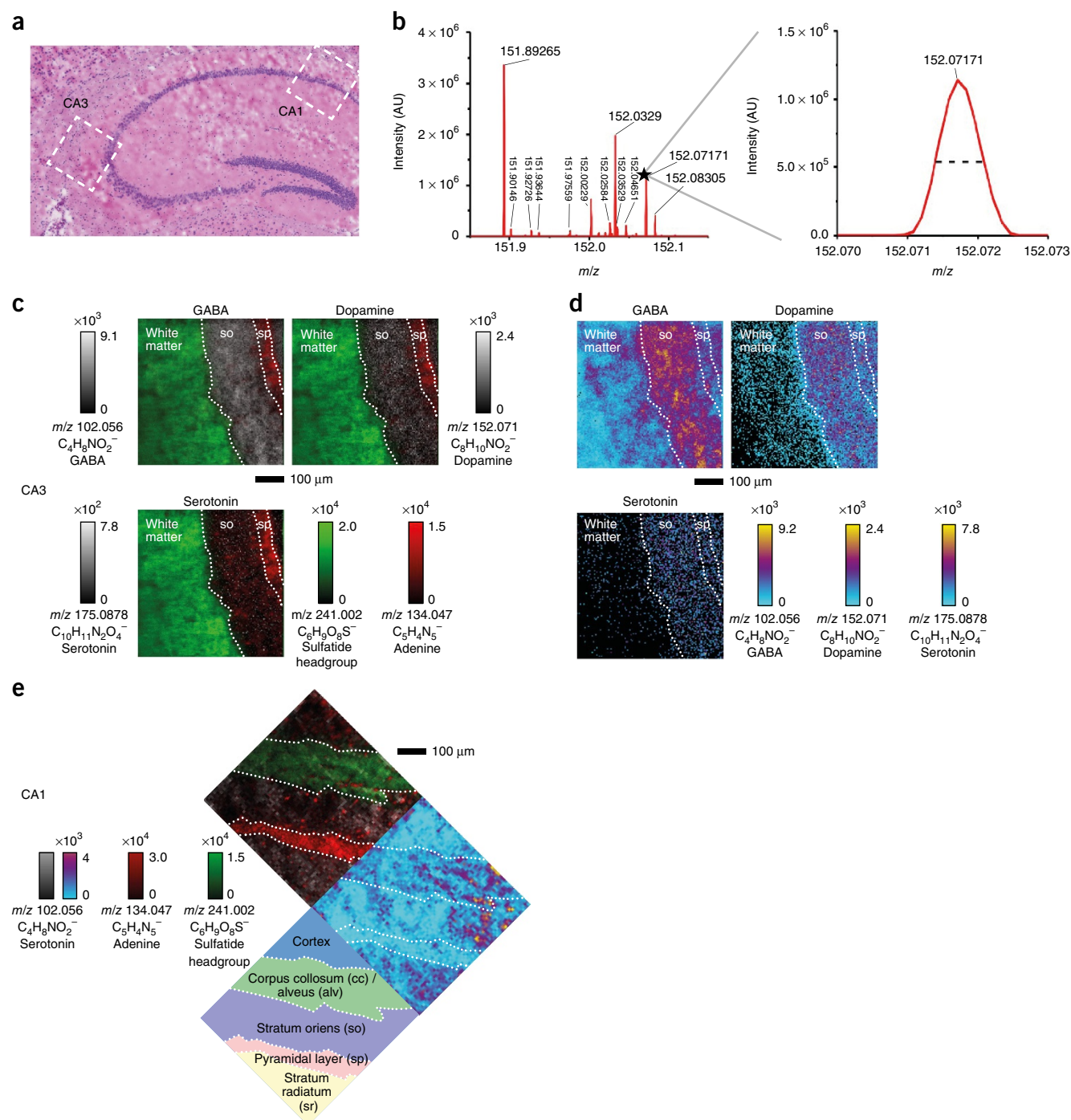


Figure 5 | Mapping of neurotransmitters in the hippocampus. **(a)** The analyzed regions in the CA1 and CA3 regions of the hippocampus are shown on the H&E-stained tissue section. **(b)** Negative ion mass spectrum (mode 7) between m/z 151.89 and m/z 152.10 showing a mass peak at m/z 152.0717 that is consistent with the deprotonated molecular ion of dopamine ($C_8H_{10}NO_2^-$) with mass accuracy (0.257 p.p.m.). **(c)** Molecular maps in the CA3 region of, clockwise, GABA or isomer, dopamine and serotonin using a gray scale overlaid with the sulfatide head group ($C_6H_9O_8S^-$, green) and adenine ($C_5H_4N_5^-$, red). **(d)** Single-ion mapping of the same neurotransmitters in a polychromatic scale showing the relative ion intensity in the anatomical regions. **(e)** Similar ion images of the CA1 region (orientated to **a**) show the distribution of GABA or isomer. All data acquired with 20 keV Ar_{3000} (lateral resolution ~ 2 μm , pixel size 1.95 μm) Orbitrap MS (mode 7). Results presented are from a single measurement.

serotonin ($C_{10}H_{11}N_2O^-$ at m/z 175.0877) were mapped in the CA3 (Fig. 5c,d) and CA1 (Fig. 5e) regions of the hippocampus. MS/MS spectra of reference samples confirmed these peaks are observed in the SIMS mass spectrum (Supplementary Fig. 13). The sub-p.p.m. mass accuracy of these peaks gives increased

accuracy of their assignment. In addition, we mapped the MS^1 -derived gas-phase fragment ions, which were identified from MS/MS reference spectra of the neurotransmitters, and found their presence and distribution to be consistent with those of the parent ions (Supplementary Fig. 13).

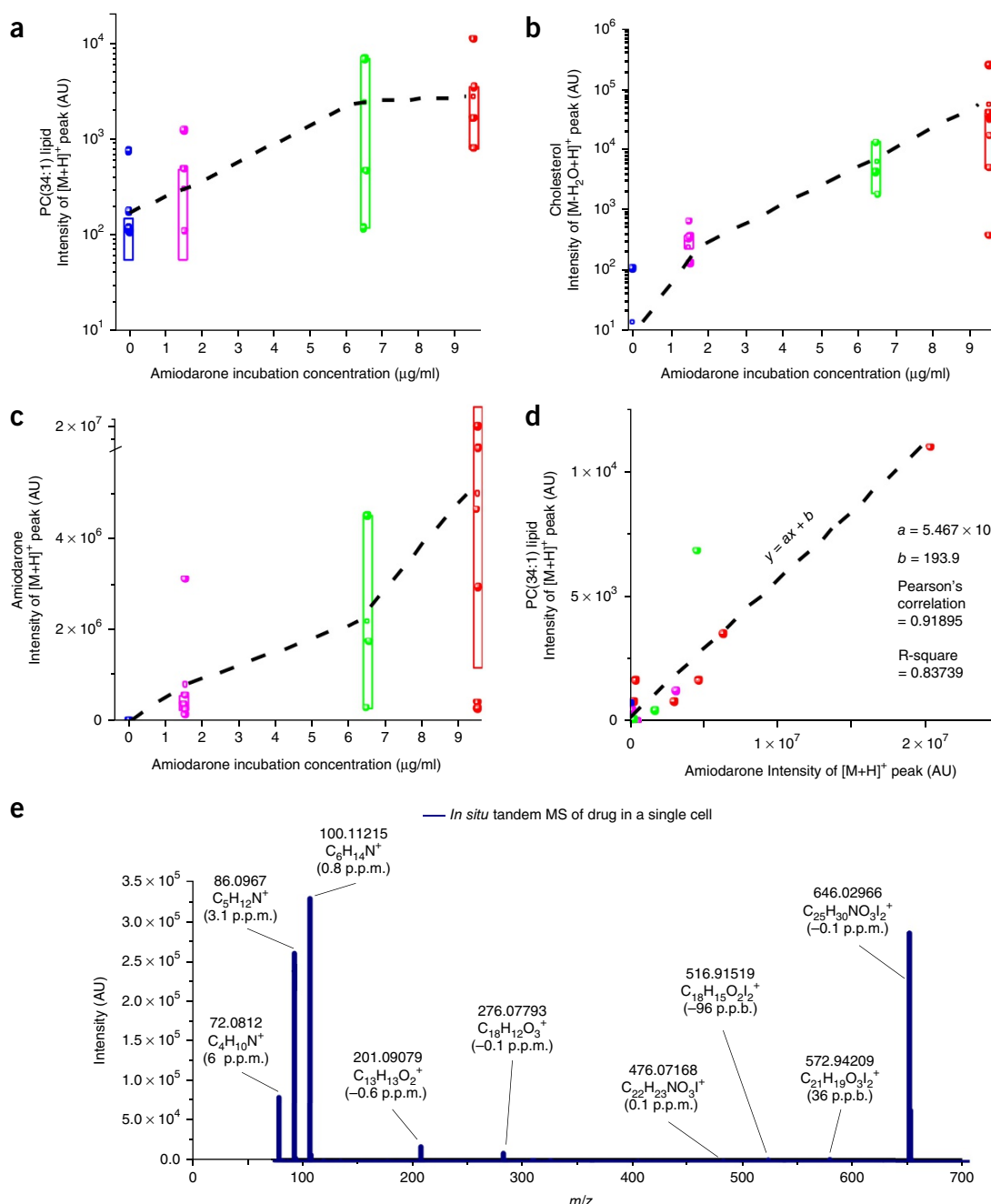


Figure 6 | Single-cell metabolomics for macrophages incubated with different concentrations of amiodarone. Dose–response curves for cells from four treatment groups, control 0 $\mu\text{g/ml}$ ($n = 8$, blue), 1.56 $\mu\text{g/ml}$ ($n = 6$, magenta), 6.25 $\mu\text{g/ml}$ ($n = 3$, green) and 9.38 $\mu\text{g/ml}$ ($n = 7$, red) incubation culture concentrations for (a) PC (34:1) at m/z 760.5848 $C_{42}H_{83}NO_8P^+$ (1.1 p.p.m.), (b) cholesterol $[M-H_2O+H]^+$ at m/z 369.3514 $C_{27}H_{45}^+$ (1.9 p.p.m.) and (c) the protonated molecular ion of the drug compound amiodarone at m/z 646.0307 $C_{25}H_{30}I_2NO_3^+$ (1.3 p.p.m.). For each plot the data points (spheres) are overlaid on a boxplot (25th quartile, median and 75th quartile), and the average (open circle) for each treatment group is connected with dotted line. (d) Scatter plot of amiodarone $[M+H]^+$ intensity with PC (34:1) $[M+H]^+$ intensity for each cell. There is a positive linear correlation (Pearson's correlation coefficient = 0.91895). (e) *In situ* MS/MS of amiodarone in a single cell. All data acquired with 20 keV Ar_{3000}^+ Orbitrap MS (mode 2).

GABA was found to be most abundant in the SO region of the hippocampus and was below detection in the SP regions in both the CA3 and CA1 ion images (Fig. 5). This finding is consistent with observations made with immunocytochemistry and electrophysiology measurements³⁰. The monoamine neurotransmitters, dopamine and serotonin, were homogeneously distributed throughout the hippocampal formation. The ability to detect alterations in the balance of tonic-based neurotransmitters with

microscopic accuracy has the potential to elucidate the effects of neuroactive substances such as antidepressants³¹ or drugs such as cocaine, which elevates dopamine levels in the hippocampus³².

Single-cell metabolic profiling

We evaluated the metabolomic profile of individual cells treated with the drug amiodarone, a cationic amphiphilic drug. At high doses and long-term usage, amiodarone (KEGG drug: D02910), a

Vaughan–Williams class III antiarrhythmic medication, is known to cause drug-induced phospholipidosis (PL)^{33–35}. PL is characterized by the prevalence of ‘foamy’ or phospholipid-laden macrophages. The exact mechanism of phospholipidosis remains the subject of debate; a number of potential contributors have been proposed. It is believed that the hydrophobic domain of amiodarone allows the molecule to cross lipid membranes, including that of the lysosome. Inside the acidic environment of the lysosome, amiodarone is hydrolyzed³⁶. The drug then accumulates in the lysosome, as this form is unable to recross the membrane. The excess drug has then been proposed to inhibit the function of the lysosomal phospholipase A2 (LPLA2, phospholipase A2 group XV)³⁷, a protein responsible for phospholipid catabolism leading to the observed phospholipid accumulation. Previously, it has been shown that ToF SIMS is able to detect the $[M+H]^+$ ion in a single rat alveolar macrophage cell²³. Recently, in a correlative NanoSIMS and electron microscopy study, the use of I^- as a chemically specific label for amiodarone and P^- as a general lipid marker illustrated amiodarone internalization in lysosomes in the same cell type and a correlated increase in lipid³⁸.

In order to evaluate the effects on the metabolic signature at the single-cell level, 3D OrbiSIMS metabolic profiles (mode 2) were acquired for cultured macrophages incubated with various concentrations of amiodarone (0, 1.56, 6.25 and 9.38 $\mu\text{g}/\text{mL}$). The average mass spectral signature (**Supplementary Fig. 14** and **Supplementary Table 9**) reveals variations in the lipid profiles among cells in the treatment groups. Metabolic changes for the intact lipid at m/z 760.5848 and putatively annotated as PC (34:1) $C_{42}H_{83}NO_8P^+$ (1.1 p.p.m.) and cholesterol $[M-H_2O+H]^+$ at m/z 369.3514 (1.9 p.p.m.) for individual cells from four amiodarone treatment groups, control 0 $\mu\text{g}/\text{mL}$ ($n = 8$, blue), 1.56 $\mu\text{g}/\text{mL}$ ($n = 6$, magenta), 6.25 $\mu\text{g}/\text{mL}$ ($n = 3$, green) and 9.38 $\mu\text{g}/\text{mL}$ ($n = 7$, red) are revealed in **Figure 6a,b**. As we expected, the amiodarone intensity per cell ($[M+H]^+$ at m/z 646.0307 $C_{25}H_{30}I_2NO_3^+$ (1.3 p.p.m.)) varies approximately linearly with incubation concentration and also demonstrates a wide range in uptake behavior at the single-cell level (**Fig. 6c**). The average PC (34:1) intensity increases over ten-fold, and the cholesterol $[M-H_2O+H]^+$ peak increases approximately exponentially with amiodarone concentration (**Fig. 6b**). This finding is consistent with previous studies following amiodarone exposure³⁹. Whilst there is a high degree of variability for individual cells in drug uptake and PC (34:1) upregulation, we see that, when intensities are shown in a correlation plot for individual cells, there is a linear correlation (Pearson's correlation coefficient = 0.91895, R square = 0.83739) (**Fig. 6d**). Such detail can only be revealed by single-cell analysis. The identification of amiodarone is confirmed from an MS/MS analysis (**Fig. 6e** and **Supplementary Fig. 15**).

DISCUSSION

The 3D OrbiSIMS enables metabolic imaging with subcellular resolution. It combines the proven power of the high-field Orbitrap for biological MS with the high-speed and high-spatial-resolution 3D imaging ToF-SIMS platform. We demonstrate a spatial resolution of under 200 nm ($172 \text{ nm} \pm 61 \text{ nm}$) ($n = 95$) simultaneously with a mass-resolving power of 355,000 for ZrO_2 nanostructures using the Bi_3 LMIG. The microfocused argon GCIB permits imaging of intact sulfatide and phosphoinositol lipids with a spatial resolution of under 2 μm simultaneously with a mass-resolving

power of >240,000 at m/z 200. A resolution of under 1.5 μm ($1.34 \mu\text{m} \pm 0.24 \mu\text{m}$) ($n = 5$) is possible for a highly skilled operator. Furthermore, a mass-resolving power of >480,000 at m/z 200 can be achieved, and this allows the fine structure of isotopic patterns to be resolved. The ability to resolve subcellular features, including the nucleus of an interneuron, is also demonstrated.

To the best of our knowledge, this represents the highest reported simultaneous spatial and mass resolutions. This provides complementary analysis to recently reported AP-MALDI imaging with 1.4- μm sampling (lateral resolution for tissue classification, 2.9 μm)⁹. Indeed, imaging of biomolecules at subcellular resolution requires a multitechnique strategy to bridge the length scales and molecular scales with the NanoSIMS 50L (CAMECA, France), which allows 50-nm resolution of elemental or stable isotope labels^{40–42} through to MALDI techniques that are able to image peptides and small proteins^{9,10}. The 3D OrbiSIMS is suited to metabolites and small molecules (<1,000 Da) and fits between these methods, enabling label-free analysis of lipid biochemistry and the role lipids play in disease pathology at subcellular resolution. Sample preparation varies significantly across these methods, with NanoSIMS requiring special care to prevent delocalization of molecules by solvents³⁸. AP-MALDI requires the least sample preparation; although, similarly, care is required not to delocalize molecules with matrix application. For 3D OrbiSIMS, care must be taken to freeze dry samples for vacuum compatibility. The instrument is also configured for cryo analysis (see Online Methods).

The application of the 3D OrbiSIMS to the single cell and its subcellular milieu will improve understanding of the location in which a drug resides and the complex responses from on-target and off-target engagement. The 3D OrbiSIMS provides rich multiplexed data sets, capturing hundreds of compounds in a single measurement with subcellular resolution. It has the potential to provide critical insight on fundamental biological processes.

METHODS

Methods, including statements of data availability and any associated accession codes and references, are available in the [online version of the paper](#).

Note: Any Supplementary Information and Source Data files are available in the online version of the paper.

ACKNOWLEDGMENTS

The authors thank N. Harrison, R. Reid, A. Harling and M. Skingle for their support during the project and T. Heller, M. Krehl, A. Dütting, P. Hörster, K. Strupat, S. Möhring, F. Czempner, A. Venckus, S. Kanngiesser, O. Lange and A. Kühn for excellent technical support. The authors also thank M. Tiddia for AFM measurement of frozen hydrated cell heights. This work forms part of the “3D nanoSIMS” project (ISG) in the Life-science and Health programme of the National Measurement System of the UK Department of Business, Energy and Industrial strategy. This work has received funding from the 3DmetChemIT project (ISG) of the EMPIR programme cofinanced by the Participating States and from the European Union's Horizon 2020 research and innovation programme.

AUTHOR CONTRIBUTIONS

M.K.P., A.P. and R.H. performed experiments. M.K.P. analyzed data. P.S.M., C.F.N. and A.W. prepared tissue and cell experiments and H & E pathology. F.K. designed continuous mode Bi LMIG. R.M., A.M., D.G., E.N. designed interface to hybridize ToF and Orbitrap spectrometers. A.P., M.K.P., R.M., A.M., E.N., R.H. optimized performance of 3D OrbiSIMS. H.A. developed computer interfacing and computational methods. R.M. and E.N. designed cryo sample handling. A.W., P.S.M. and C.T.D. direction of pharmaceutical studies. M.R.A., S.H. and E.N. gave technical leadership at Thermo Fisher Scientific and ION-TOF, respectively. I.S.G.

original design concept and supervised the project. M.K.P. and I.S.G. wrote the paper. All authors read and commented on the paper.

COMPETING FINANCIAL INTERESTS

The authors declare competing financial interests: details are available in the online version of the paper.

Reprints and permissions information is available online at <http://www.nature.com/reprints/index.html>. Publisher's note: Springer Nature remains neutral with regard to jurisdictional claims in published maps and institutional affiliations.

- Elowitz, M.B., Levine, A.J., Siggia, E.D. & Swain, P.S. Stochastic gene expression in a single cell. *Science* **297**, 1183–1186 (2002).
- Zenobi, R. Single-cell metabolomics: analytical and biological perspectives. *Science* **342**, 1243259 (2013).
- Rubakhin, S.S., Lanni, E.J. & Sweedler, J.V. Progress toward single cell metabolomics. *Curr. Opin. Biotechnol.* **24**, 95–104 (2013).
- Passarelli, M.K. & Ewing, A.G. Single-cell imaging mass spectrometry. *Curr. Opin. Chem. Biol.* **17**, 854–859 (2013).
- Scannell, J.W., Blanckley, A., Boldon, H. & Warrington, B. Diagnosing the decline in pharmaceutical R&D efficiency. *Nat. Rev. Drug Discov.* **11**, 191–200 (2012).
- Dollery, C.T. Intracellular drug concentrations. *Clin. Pharmacol. Ther.* **93**, 263–266 (2013).
- Makarov, A. Electrostatic axially harmonic orbital trapping: a high-performance technique of mass analysis. *Anal. Chem.* **72**, 1156–1162 (2000).
- Hu, Q. *et al.* The Orbitrap: a new mass spectrometer. *J. Mass Spectrom.* **40**, 430–443 (2005).
- Kompauer, M., Heiles, S. & Spengler, B. Atmospheric pressure MALDI mass spectrometry imaging of tissues and cells at 1.4- μ m lateral resolution. *Nat. Methods* **14**, 90–96 (2017).
- Zavalin, A., Yang, J., Hayden, K., Vestal, M. & Caprioli, R.M. Tissue protein imaging at 1 μ m laser spot diameter for high spatial resolution and high imaging speed using transmission geometry MALDI TOF MS. *Anal. Bioanal. Chem.* **407**, 2337–2342 (2015).
- Fletcher, J.S. *et al.* A new dynamic in mass spectral imaging of single biological cells. *Anal. Chem.* **80**, 9058–9064 (2008).
- Fletcher, J.S. & Vickerman, J.C. A new SIMS paradigm for 2D and 3D molecular imaging of bio-systems. *Anal. Bioanal. Chem.* **396**, 85–104 (2010).
- Lee, J.L.S. *et al.* Organic depth profiling of a nanostructured delta layer reference material using large argon cluster ions. *Anal. Chem.* **82**, 98–105 (2010).
- Körsgen, M., Pelster, A., Dreisewerd, K. & Arlinghaus, H.F. 3D ToF-SIMS analysis of peptide incorporation into MALDI matrix crystals with sub-micrometer resolution. *J. Am. Soc. Mass Spectrom.* **27**, 277–284 (2016).
- Carado, A. *et al.* C60 secondary ion mass spectrometry with a hybrid-quadrupole orthogonal time-of-flight mass spectrometer. *Anal. Chem.* **80**, 7921–7929 (2008).
- Bruinen, A.L., Fisher, G.L. & Heeren, R.M.A. In *Imaging Mass Spectrometry: Methods and Protocols* (ed. Cole, L.M.) 165–173 (Springer, 2017).
- Marshall, A.G., Hendrickson, C.L. & Jackson, G.S. Fourier transform ion cyclotron resonance mass spectrometry: a primer. *Mass Spectrom. Rev.* **17**, 1–35 (1998).
- Maharrey, S. *et al.* High mass resolution SIMS. *Appl. Surf. Sci.* **231–232**, 972–975 (2004).
- Smith, D.F., Robinson, E.W., Tolmachev, A.V., Heeren, R.M.A. & Paša-Tolić, L. C60 secondary ion Fourier transform ion cyclotron resonance mass spectrometry. *Anal. Chem.* **83**, 9552–9556 (2011).
- Scheltema, R.A. *et al.* The Q Exactive HF, a Benchtop mass spectrometer with a pre-filter, high-performance quadrupole and an ultra-high-field Orbitrap analyzer. *Mol. Cell. Proteomics* **13**, 3698–3708 (2014).
- Michalski, A. *et al.* Mass spectrometry-based proteomics using Q Exactive, a high-performance benchtop quadrupole orbitrap mass spectrometer. *Mol. Cell. Proteomics* **10**, M111.011015 (2011).
- Seah, M.P., Havelund, R. & Gilmore, I.S. Universal equation for argon cluster size-dependence of secondary ion spectra in SIMS of organic materials. *J. Phys. Chem. C* **118**, 12862–12872 (2014).
- Passarelli, M.K. *et al.* Single-cell analysis: visualizing pharmaceutical and metabolite uptake in cells with label-free 3D mass spectrometry imaging. *Anal. Chem.* **87**, 6696–6702 (2015).
- Andersen, P. *et al.* (eds.) *The Hippocampus Book* (Oxford University Press, 2006).
- Burgess, N., Maguire, E.A. & O'Keefe, J. The human hippocampus and spatial and episodic memory. *Neuron* **35**, 625–641 (2002).
- O'Keefe, J. & Dostrovsky, J. The hippocampus as a spatial map. Preliminary evidence from unit activity in the freely-moving rat. *Brain Res.* **34**, 171–175 (1971).
- Jones, A.R., Overly, C.C. & Sunkin, S.M. The Allen Brain Atlas: 5 years and beyond. *Nat. Rev. Neurosci.* **10**, 821–828 (2009).
- Fletcher, J.S., Rabbani, S., Henderson, A., Lockyer, N.P. & Vickerman, J.C. Three-dimensional mass spectral imaging of HeLa-M cells—sample preparation, data interpretation and visualisation. *Rapid Commun. Mass Spectrom.* **25**, 925–932 (2011).
- Jeon, S.-B., Yoon, H.J., Park, S.-H., Kim, I.-H. & Park, E.J. Sulfatide, a major lipid component of myelin sheath, activates inflammatory responses as an endogenous stimulator in brain-resident immune cells. *J. Immunol.* **181**, 8077–8087 (2008).
- Yanovsky, Y., Sergeeva, O.A., Freund, T.F. & Haas, H.L. Activation of interneurons at the stratum oriens/alveus border suppresses excitatory transmission to apical dendrites in the CA1 area of the mouse hippocampus. *Neuroscience* **77**, 87–96 (1997).
- Santarelli, L. *et al.* Requirement of hippocampal neurogenesis for the behavioral effects of antidepressants. *Science* **301**, 805–809 (2003).
- Kramar, C.P., Chefer, V.I., Wise, R.A., Medina, J.H. & Barbano, M.F. Dopamine in the dorsal hippocampus impairs the late consolidation of cocaine-associated memory. *Neuropsychopharmacology* **39**, 1645–1653 (2014).
- Papiris, S.A., Triantafyllidou, C., Kolilekas, L., Markoulaki, D. & Manali, E.D. Amiodarone: review of pulmonary effects and toxicity. *Drug Saf.* **33**, 539–558 (2010).
- Anderson, N. & Borlak, J. Drug-induced phospholipidosis. *FEBS Lett.* **580**, 5533–5540 (2006).
- Mesens, N. *et al.* Phospholipidosis in rats treated with amiodarone: serum biochemistry and whole genome micro-array analysis supporting the lipid traffic jam hypothesis and the subsequent rise of the biomarker BMP. *Toxicol. Pathol.* **40**, 491–503 (2012).
- Shayman, J.A. & Abe, A. Drug induced phospholipidosis: an acquired lysosomal storage disorder. *Biochim. Biophys. Acta* **1831**, 602–611 (2013).
- Abe, A. & Shayman, J.A. The role of negatively charged lipids in lysosomal phospholipase A2 function. *J. Lipid Res.* **50**, 2027–2035 (2009).
- Jiang, H. *et al.* High-resolution sub-cellular imaging by correlative NanoSIMS and electron microscopy of amiodarone internalisation by lung macrophages as evidence for drug-induced phospholipidosis. *Chem. Commun. (Camb.)* **53**, 1506–1509 (2017).
- Lakhdar, A.A., Farish, E., Hillis, W.S. & Dunn, F.G. Long-term amiodarone therapy raises serum cholesterol. *Eur. J. Clin. Pharmacol.* **40**, 477–480 (1991).
- Zhang, D.S. *et al.* Multi-isotope imaging mass spectrometry reveals slow protein turnover in hair-cell stereocilia. *Nature* **481**, 520–524 (2012).
- Kraft, M.L., Weber, P.K., Longo, M.L., Hutcheon, I.D. & Boxer, S.G. Phase separation of lipid membranes analyzed with high-resolution secondary ion mass spectrometry. *Science* **313**, 1948–1951 (2006).
- Lovrić, J. *et al.* Nano secondary ion mass spectrometry imaging of dopamine distribution across nanometer vesicles. *ACS Nano* **11**, 3446–3455 (2017).

ONLINE METHODS

Sample preparation. We prepared mouse brain tissue sections using the following procedure. All animal studies were ethically reviewed and carried out in accordance with Animals (Scientific Procedures) Act 1986 and the GSK Policy on the Care, Welfare and Treatment of Animals. Female CD-1 mice, typically 6–8 weeks old, were sacrificed by Schedule 1 method. The brains were quickly extracted and frozen in dry ice. The intact brains were stored at -80°C until sectioning. Coronal tissue sections were cut with a thickness of $10\text{ }\mu\text{m}$ using a Leica CM3050S cryostat (Leica, Germany) at -22°C . The brain sections were thaw mounted on conductive indium tin oxide (ITO) glass slides (Bruker, Germany) and stored at -80°C until further use.

SIMS analysis and histological haematoxylin and eosin (H&E) staining were performed on the adjacent tissue sections. The tissue was stained using a Leica ST5020 autostainer (Leica, Germany) using standard H&E protocol at GlaxoSmithKline. The stained sections were cover slipped with a xylene-based mountant using a Leica CV5030 coverslipper (Leica, Germany). Optical images of the H&E-stained tissue sections were obtained with a Hamamatsu Nanozoomer 2.0 HT microscope with $20\times$ magnification (Hamamatsu Photonics, Japan). Haematoxylin (Mayer) and eosin (1% aqueous) were obtained from Pioneer Research Chemicals Ltd (Essex, UK). The solvents, xylenes (ACS reagent $>98.5\%$, xylenes + ethylbenzene basis) and denatured ethanol (UK IDA Standard) were obtained from Sigma-Aldrich (Saint Louis, Missouri, USA).

Reference samples of lipid and neurotransmitters were prepared as follows. C24:1 Mono-Sulfo Galactosyl(β) Ceramide (d18:1/24:1) (Avanti Polar Lipids, USA, CAS 1246355-69-0, purity $>99\%$) was drop deposited onto a clean silicon wafer from a 1:1 by volume methanol:chloroform solvent mixture. Reference samples of gamma-aminobutyric acid (GABA) (Sigma-Aldrich, USA, CAS 56-12-2, purity $\geq 99\%$), dopamine (Sigma-Aldrich, USA, CAS 62-31-7) and serotonin (Sigma-Aldrich, USA, CAS 50-67-9, purity $\geq 98\%$) were prepared similarly. A reference sample of 1,2-dilauroyl-sn-glycero-3-phosphoethanolamine (Avanti Polar Lipids, USA, CAS 59752-57-7, purity $>99\%$) was prepared by pressing sample powder directly onto a previously cleaned silicon wafer using a clean metal spatula.

Single-cell studies used NR8383 cells (ATCC CRL-2192, Manassas, Virginia, USA), an immortalized cell line derived from a lung macrophage (Sprague–Dawley rat). The cells were tested for mycoplasma within GlaxoSmithKline and are not listed in the database of commonly misidentified cell lines. These were grown on indium tin oxide (ITO) glass slides (Bruker, Germany) with Ham's F-12 Nutrient Mixture media containing GlutaMax and Phenol Red (Gibco, USA) and 15% dialyzed, heat-inactivated FBS (Gibco, USA). 5 mg/mL stock solutions of amiodarone hydrochloride (Sigma-Aldrich, CAS 19774-82-4, purity 98%) were prepared in 50:50 water:MeOH. The stock solutions were added to the growth media for final media concentrations of 1.56 $\mu\text{g/mL}$, 6.25 $\mu\text{g/mL}$ and 9.38 $\mu\text{g/mL}$. The cells were incubated (5% CO_2 and 37°C) in all of the listed concentrations in the drug-containing media for 72 h. Control cells were incubated alongside the dosed cells. To prepare the cells for analysis in the 3D OrbiSIMS, the media were removed, and the cells were washed three times with 150 mM ammonium formate solution (Sigma-Aldrich, USA). This removes salts that cause unwanted signal

suppression in SIMS. The cells were frozen and dried under vacuum (Genevac, USA) and stored at -80°C until analysis. Before SIMS analysis, the samples were warmed to room temperature in a vacuum chamber. The cells for **Figure 2** were prepared using the same method in the same laboratory by the same person, but at a later date.

To demonstrate nanoscale resolution using the Bi LMIG simultaneously with high mass resolution using the Orbitrap MS, a sample of zirconium dioxide (ZrO_2) nanostructures was prepared. ZrO_2 nanoparticles were dispersed in aqueous solution and spotted onto a clean Al foil. During evaporation, crystals formed that were heterogeneous in size and exhibited nanoscale features. For evaluation of the 3D imaging capability, the NPL Organic Multilayer (OML) reference sample was used (NPL, UK). The reference sample consists of layers of Irganox 1010 and Irganox 3114 deposited onto a Si substrate to form four 1 nm thick layers of Irganox 3114 placed at depths of 50 nm, 100 nm, 200 nm, and 300 nm in a 400 nm Irganox 1010 film.

3D OrbiSIMS instrumentation. The instrument uses a Q Exactive HF for Orbitrap MS. In the Orbitrap MS modes (**Fig. 1**) a quasicontinuous primary ion beam is used for secondary-ion generation without affecting the mass resolution. This is due to the intermediate trapping capabilities of the Orbitrap for the secondary ion beam. Tandem MS, also known as MS/MS, operates in the same way as a Q Exactive HF. In this mode, the quadrupole mass filter isolates the precursor ions, and the ions are fragmented in the higher energy collisional dissociation (HCD) collision cell (with nitrogen gas, 0–100 eV collision energy). The fragment ions are transferred to the C-trap and orthogonally injected into the Orbitrap cell to produce MS/MS spectra with full mass resolution and mass accuracy. The MS/MS capability and the high mass-resolving power of the Orbitrap analysis improve signal to noise and researchers' ability to detect low-abundance ions that may be obscured by nearby ions of higher intensity.

In ToF MS modes, short ($<\text{ns}$) primary ion pulses generate secondary ions which are accelerated from the sample surface into the ToF analyzer. In all SIMS experiments (both ToF MS and Orbitrap MS) an extraction potential of 2,000 V is used (opposite polarity to the secondary ion). The measurement principle of the ToF requires either short primary ion pulses or, if longer primary ion pulses ($<200\text{ ns}$) are applied, a pulsed and delayed extraction of the mass analyzer extraction electrode to obtain good mass resolution. Because of the very different ion-detection systems (ToF MS uses single-ion counting, and Orbitrap MS uses image current detection and Fourier transformation), the numerical values of the resulting signal intensities cannot be compared one to one. For the Orbitrap MS results, a conversion factor must be determined in order to calculate the number of ions detected.

The 3D OrbiSIMS is equipped with a newly developed 30 keV bismuth cluster Bi LMIG (Bi Nanoprobe, ION-TOF GmbH) with a lateral resolution of $<200\text{ nm}$ (**Supplementary Fig. 6**). The ion gun operates with selected cluster species (e.g., Bi_3^+) in a quasicontinuous (DC) mode using a Wien filter. In combination with the ToF mass analyzer, 0.6 ns long ion pulses are usually achieved if bunching is applied. Longer pulse durations of 1.5–150 ns can be obtained in unbunched operation. In addition, a new 20 keV argon GCIB provides a focused beam of Ar clusters with $<2\text{ }\mu\text{m}$ lateral resolution imaging (**Supplementary Fig. 5**). For the GCIB,

the size of the virtual source is larger than that of the Bi LMIG, and this makes it technically more demanding to get to a small focal spot size. In order to improve the focal spot size of the gas cluster ion source, the ion optical demagnification of the ion column was increased by optimization of the electrostatic lenses. Additionally, an aperture was introduced in order to block larger beam angles, thereby reducing aberration effects. The loss of beam current is more than compensated for by operating the ion beam in a quasi-continuous mode for combination with the Orbitrap MS. By taking these measures, it was possible to decrease the spot size to below 2 μm with a current of more than 30 pA, and Orbitrap MS images with a resolution of <2 μm could be achieved.

The 3D OrbiSIMS can accommodate a large analysis area (up to the size of the sample holder, 100 mm \times 70 mm). Its field of view and lateral resolution are ultimately limited by the acquisition time and the size of the data file. Details of the GCIB with Orbitrap MS imaging mode 7 are provided in the **Supplementary Protocol**⁴³. The instrument has cryogenic sample cooling in both the analysis and preparation chamber (sample temperature < -130 °C (143 K)) with a Leica VCT 500 (Leica, Germany) sample-transfer system compatible with cryo-s.e.m. and cryo-TEM instruments.

Reproducibility testing. To improve reproducibility between operators, we use mouse brain tissue samples from the same batch for training purposes and validation of the instrument performance. Images with the same spatial resolution and mass-resolving power can be reproduced. To help with reproducibility, we include in the **Supplementary Protocol**⁴³ an author outside of this study. Reproducibility between instruments is not yet tested, as this is currently the only instrument.

3D OrbiSIMS experimental methods. Mass calibration of the Q Exactive instrument was performed once a day using silver cluster ions. Mass calibration of the ToF was performed using the same ions. For the 3D single-cell image (mode 10) in **Figure 2**, the high-lateral-resolution images were obtained with 30 keV Bi_3^+ LMIG (approximately 300 nm resolution) from an analysis area of 100 μm \times 100 μm using the ToF MS. These images are interleaved by Orbitrap MS acquired during the 20 keV Ar_{3000}^+ GCIB sputtering cycle from the same field of view, but with an additional sputter border of 20 μm width to avoid edge effects. 50 scans were accumulated in the ToF images, which corresponded to a total primary ion dose of 3.3×10^{12} ions/ cm^2 . The total GCIB sputtering dose was 1.1×10^{15} ions/ cm^2 . The cell height is estimated from AFM topographic images, Asylum MFP-3D (Asylum Research, USA), of four cells from the same sample post exposure to the 3D OrbiSIMS vacuum. The average cell height is $2.04 \mu\text{m} \pm 0.23 \mu\text{m}$ ($\mu \pm 1\sigma$) $n = 4$ (2.04 μm , 2.23 μm , 2.18 μm , 1.71 μm). In **Figures 3–5**, the coronal tissue section was imaged with a focused 20 keV Ar_{3000}^+ ion source (in **Fig. 4**, 20 keV Ar_{2500}^+) with the Orbitrap MS (mode 7). A step-by-step protocol for label-free imaging of biomolecules, including lipids and neurotransmitters, in murine brain sections using the 3D OrbiSIMS is provided in the **Supplementary Protocol**⁴³. An ion image containing 256 \times 256 pixels was acquired over an area of 500 μm \times 500 μm (pixel size = 1.95 μm \times 1.95 μm). Approximately 2,300 shots at 240 μs per cycle were accumulated in the C-trap per pixel. The Orbitrap analyzer was operated in negative- and positive-ion mode at the 240,000 at m/z 200 mass resolution setting (512 ms transient

time). Mass spectra information was collected for a mass range from 60 to 1,000 Da. The total ion dose was 2.0×10^{15} ions/ cm^2 . The total ion image-acquisition time was approximately 10 h. Fast-imaging survey image of the hippocampus formation was obtained with a pulsed 30 keV Bi_3^+ ion beam and the ToF mass analyzer (mode 6). Stage and ion beam rastering were used to image the 3.5 mm \times 2.3 mm analysis area (pixel size = 2 μm ; ion images down binned to 8 μm by combining adjacent pixels). The fast ToF MS image was acquired in negative-ion mode, and acquisition took approximately 36 min. The total ion dose was 4.2×10^{10} ions/ cm^2 . The mass-resolving power of the image was approximately 5,000 at m/z 200. In **Figure 3d**, the spectrum is for 15 pixels defined by an intensity threshold of $>2.7 \times 10^3$ with a background spectrum subtracted. The background spectrum was obtained by summing 15 pixels in the SO region of the ion image, where the adenine signal is absent. The tandem MS spectrum in **Figure 4a** was obtained using a 10 keV argon cluster beam. The collisional cell energy was set to 65 V. The spectra were accumulated for 60 s as the ion beam rastered in a random pattern in the CC region of the brain section. The tandem MS spectrum of a cholesterol (**Supplementary Fig. 2**) at m/z 369.3509 was acquired with a collision energy of 30 eV from the corpus callosum of a coronal mouse brain section, where it was found in abundance. The mass spectrum was taken at full mass-resolving power and summed over 60 s.

We acquired metabolic profiles of amiodarone-dosed cells (**Fig. 6**) using a 20 keV Ar_{3000}^+ ion beam and the Orbitrap MS (mode 2). Spectra were summed across an analysis area of 20 μm \times 20 μm until the entire cell was consumed. The Orbitrap analyzer was operated in positive-ion mode at the 240,000 at m/z 200 mass-resolution setting (512 ms transient time). Mass spectra information was collected for a mass range from 60 to 1,000 Da. The total ion dose ranged from 1.3×10^{14} to 7.8×10^{14} ions/ cm^2 .

To demonstrate the capability of the 3D OrbiSIMS for depth profiling and 3D imaging, we obtained negative-ion data from the NPL organic multilayer reference material for three modes: mode 3 (single beam, 5 keV Ar_{2000}^+ , Orbitrap MS); mode 9 (analysis with 30 keV Bi_3 and ToF MS, sputtering 5 keV Ar_{2000}^+) and mode 10 (5 keV Ar_{2000}^+ sputtering and Orbitrap MS analysis and 30 keV Bi_3 with ToF MS imaging). For all three modes, a 5 keV Ar_{2000}^+ beam with a current of 41 pA was used for sputtering a 250 μm \times 250 μm region of the sample. The beam is defocused to a spot size of 20 μm . Electrons with an energy of 21 eV and a current of 10 μA were used for charge compensation. In operational modes 3 and 10, secondary ions sputtered by the Ar_{2000}^+ beam from the central 130 μm \times 130 μm of the crater were analyzed using the Orbitrap spectrometer. In the dual-beam modes, modes 9 and 10, secondary ion images with 128 \times 128 pixels were obtained from the central 130 μm \times 130 μm of the crater using a pulsed 30 keV Bi_3^+ with a beam current of 0.05 pA and using the ToF analyzer. These dual-beam experiments were carried out in the noninterlaced mode. In mode 9, the sample was sputtered using the Ar_{2000}^+ beam for 2.0 s per cycle and imaged using the Bi_3^+ beam for 3.28 s. The ion dose ratio was 0.7% (Bi_3^+ to Ar_{2000}^+). In mode 10, the sample was sputtered for 7.5 s per cycle, which gave a dose ratio of 0.2%. The depth resolution is measured as the full width at half maximum of the m/z 564 delta layer peaks.

Data analysis. The 3D OrbiSIMS was controlled by software provided by SurfaceLab Version 6.7 (ION-TOF, Germany), which

used the application programming interface (API) provided by Thermo Fisher for both control of the Orbitrap MS portion of the instrument as well as online retrieval of the data. Both ToF-SIMS and Orbitrap MS image analyses were performed using SurfaceLab Version 6.7 (ION-TOF, Germany), OriginPro 2016 and MATLAB 2016a. Chemical structures were drawn in ChemDraw 14.0.

All Orbitrap MS images, depth profiles and linescans were created with a tolerance between ± 2 and ± 15 p.p.m., depending on the width of the signal peak, which increases proportional to the square root of its mass. This is the reciprocal of the resolving power at a given mass $\times 10^6$. The resolving power is plotted in **Supplementary Figure 1b**.

In **Figure 2**, the ToF-SIMS ion images for m/z 184, 157 and 646 were smoothed with a smoothing filter (average 1, ION-TOF SurfaceLab). 3D renderings were constructed using an isosurface visualization for m/z 184 with a 7.2% isovalue, 40% opacity, xy binning of 16 pixels and z binning of four scans. For the nuclear marker, m/z 157, and amiodarone $[M+H]^+$, m/z 646, a so-called volume visualization using a threshold at 15% with the same binning using SurfaceLab Version 6.7 (ION-TOF, Germany). The 3D image was created after the z position of the voxels was adjusted to take the initial sample topography into account, under the assumption that the indium tin oxide substrate is a uniform flat plane⁴⁴.

Statistical analysis. Samples were not randomized. The biological samples are included to demonstrate the new capabilities of the OrbiSIMS method rather than specific and comprehensive biological studies. The investigators were not blinded to group allocation.

The resolution of the GCIB beam was measured by imaging an electroformed mesh grid from the ion-induced secondary electron image (**Supplementary Fig. 3a**). To achieve a reliable measurement, the lateral resolution was measured from 246 line scans across the edge of the grid in different locations spread over $4.7\ \mu\text{m}$ for both the x -axis and y -axis (**Supplementary Fig. 3b,c**). The FWHM of the ion beam profile (lateral resolution) is determined from the distance interval between the 88% to 12% intensities of an error function fit to the linescan across the edge. The resolution measurements are fitted to a normal distribution with a mean and s.d. of $1.72\ \mu\text{m} \pm 0.24\ \mu\text{m}$ ($n = 246$) across the x -axis and $1.04\ \mu\text{m} \pm 0.16\ \mu\text{m}$ ($n = 246$) across the y -axis (**Supplementary Fig. 3d**). The difference in the x -axis and y -axis FWHM lateral resolution measurements is due to the 45° angle of incidence along the x -axis (**Supplementary Fig. 3**). The same procedure was conducted with the secondary ion extraction potential on (needed for ion detection) and resolution degrades with the ion-extraction optics (**Supplementary Fig. 4**). The average FWHM lateral resolution was $2.49\ \mu\text{m} \pm 0.36\ \mu\text{m}$ ($\mu \pm 1\sigma$) ($n = 243$, gray bars) across the x -axis and $1.84\ \mu\text{m} \pm 0.36\ \mu\text{m}$ ($\mu \pm 1\sigma$) ($n = 254$, red bars) across

the y -axis. For a practical measurement of the resolution in tissue imaging, five measurements are made from the intensity line scan of summed intensity of nuclear markers C_4N_3^- at m/z 90.0095 (2.8 p.p.m.), $\text{CN}_2\text{O}_2\text{P}^-$ at m/z 102.9702 (0.6 p.p.m.), $\text{C}_4\text{H}_2\text{N}_4^-$ at m/z 106.0285 (0.3 p.p.m.), $\text{C}_4\text{H}_3\text{N}_4^-$ at m/z 107.0207 (0.2 p.p.m.), C_5HN_4^- at m/z 117.0207 (0.2 p.p.m.), $\text{C}_5\text{H}_3\text{N}_4^-$ at m/z 119.0363 (0.3 p.p.m.), $\text{C}_5\text{HN}_4\text{O}^-$ at m/z 133.0156 (0.1 p.p.m.) and $\text{C}_5\text{H}_4\text{N}_5^-$ at m/z 134.0472 (-0.1 p.p.m.). The mean and s.d. values are $1.34\ \mu\text{m} \pm 0.24\ \mu\text{m}$ ($n = 5$).

The spatial resolution for the 30 kV Bi_3^{2+} LMIG was determined using the ZrO_2 nanostructures shown in the total ion image (**Supplementary Fig. 6a**) and the ZrO^+ image (**Supplementary Fig. 6b**). We acquired a high-resolution secondary electron image (**Supplementary Fig. 6c**) and ion image (**Supplementary Fig. 6d**) from a $20\ \mu\text{m} \times 20\ \mu\text{m}$ region with a pixel size of 78 nm. As previously noted, 95 y -axis linescans of the total ion intensity across the edge of the crystal were acquired (**Supplementary Fig. 6e**). Measurements were taken over a length of $1.5\ \mu\text{m}$. A normal distribution was fitted to the population to give the mean and s.d. of $172\ \text{nm} \pm 61\ \text{nm}$ ($\mu \pm 1\sigma$) ($n = 95$). The bismuth ion gun was operated at 60 μs per cycle and 1,800 shots per pixel. The secondary ions were collected in the C-trap for 500 ms before being injected into the Orbitrap analyzer. The trap was operated in positive-ion mode at the 240,000 at m/z 200 mass-resolution setting. The total ion dose was 4.28×10^{16} ions/ cm^2 . The total acquisition time of the ion image was approximately 9 h.

The single-cell drug accumulation and lipid upregulation (**Fig. 6d**) correlation calculations were performed in OriginPro software (2015; OriginLab, Massachusetts, USA). The correlation test was performed using a Pearson's (two-tailed) correlation test at the 95% confidence level.

A Life Sciences Reporting Summary is provided.

Data availability statement. The data that support the findings of this study are available in figshare at <http://dx.doi.org/10.6084/m9.figshare.5459680>. We provide the Orbitrap data in the mzML format for spectra and the ImzML format for images. The ToF image in **Figure 2** is in the GRD data (ToF-SIMS generic raw data) format. Data may be opened using Spectral Analysis software⁴⁵ available from Github: <https://github.com/AlanRace/SpectralAnalysis>.

43. Havelund, R. *et al.* Label-free imaging of biomolecules in murine brain sections using the 3D OrbiSIMS. *Protocol Exchange* <https://doi.org/10.1038/protex.2017.120> (2017).
44. Robinson, M.A., Graham, D.J. & Castner, D.G. ToF-SIMS depth profiling of cells: z -correction, 3D imaging, and sputter rate of individual NIH/3T3 fibroblasts. *Anal. Chem.* **84**, 4880–4885 (2012).
45. Race, A.M. *et al.* SpectralAnalysis: software for the masses. *Anal. Chem.* **88**, 9451–9458 (2016).

Life Sciences Reporting Summary

Nature Research wishes to improve the reproducibility of the work that we publish. This form is intended for publication with all accepted life science papers and provides structure for consistency and transparency in reporting. Every life science submission will use this form; some list items might not apply to an individual manuscript, but all fields must be completed for clarity.

For further information on the points included in this form, see [Reporting Life Sciences Research](#). For further information on Nature Research policies, including our [data availability policy](#), see [Authors & Referees](#) and the [Editorial Policy Checklist](#).

► Experimental design

1. Sample size

Describe how sample size was determined.

In this study the measure of the spatial resolution for inorganics and organics is where special care is needed for meaningful measurement. To do this we have provided extensive data in the supporting information. For inorganics we have $n = 95$ and report the mean and standard deviation. We also show the histogram of measurements with the fitted normal distribution. We have also used the Full Width at Half Maximum measure of resolution. For the measurement of spatial resolution of the GCIB we follow a similar method with $n=243$ using a grid. To demonstrate the resolution in a biological sample 5 measurements of the FWHM resolution from 2 nuclei are obtained. In Fig 6, the number of single cell measurements is limited by acquisition time.

2. Data exclusions

Describe any data exclusions.

No data is excluded. Following the reviewers helpful comments we have acquired additional validation data for GABA, dopamine and serotonin from pure compounds. In addition, we show the MS/MS spectra and that the secondary ion image for these is correlated with the image for the identified ions. This gives the additional confidence required by the reviewers. We do not have this confirmation data for glutamate and so do not show that in Fig 5. The data is there and is not excluded.

3. Replication

Describe whether the experimental findings were reliably reproduced.

Reproducibility between operators: We now use mouse brain tissue samples from the same batch for training purposes and validation of the instrument performance. Images with the same spatial resolution and mass resolving power can be reproduced. Reproducibility between instruments: This is not yet tested as this is currently the only instrument. To help with reproducibility, we include in the supplementary protocol an author outside of this publication.

4. Randomization

Describe how samples/organisms/participants were allocated into experimental groups.

Samples were not randomised. The biological samples are included to demonstrate the new capabilities with the OrbiSIMS method rather than specific and comprehensive biological studies.

5. Blinding

Describe whether the investigators were blinded to group allocation during data collection and/or analysis.

Investigators were not blinded to group allocation.

Note: all studies involving animals and/or human research participants must disclose whether blinding and randomization were used.

6. Statistical parameters

For all figures and tables that use statistical methods, confirm that the following items are present in relevant figure legends (or in the Methods section if additional space is needed).

n/a Confirmed

- ☐ ☒ The exact sample size (n) for each experimental group/condition, given as a discrete number and unit of measurement (animals, litters, cultures, etc.)
- ☐ ☒ A description of how samples were collected, noting whether measurements were taken from distinct samples or whether the same sample was measured repeatedly
- ☐ ☒ A statement indicating how many times each experiment was replicated
- ☐ ☒ The statistical test(s) used and whether they are one- or two-sided (note: only common tests should be described solely by name; more complex techniques should be described in the Methods section)
- ☐ ☒ A description of any assumptions or corrections, such as an adjustment for multiple comparisons
- ☐ ☒ The test results (e.g. P values) given as exact values whenever possible and with confidence intervals noted
- ☐ ☒ A clear description of statistics including central tendency (e.g. median, mean) and variation (e.g. standard deviation, interquartile range)
- ☐ ☒ Clearly defined error bars

See the web collection on [statistics for biologists](#) for further resources and guidance.

► Software

Policy information about [availability of computer code](#)

7. Software

Describe the software used to analyze the data in this study.

Software used: ION-TOF SurfaceLab Version 6.7, OriginPro 2016 and MATLAB 2016a. We also used our own publicly available software, SpectralAnalysis (available at <https://github.com/AlanRace/SpectralAnalysis>)

For manuscripts utilizing custom algorithms or software that are central to the paper but not yet described in the published literature, software must be made available to editors and reviewers upon request. We strongly encourage code deposition in a community repository (e.g. GitHub). *Nature Methods* [guidance for providing algorithms and software for publication](#) provides further information on this topic.

► Materials and reagents

Policy information about [availability of materials](#)

8. Materials availability

Indicate whether there are restrictions on availability of unique materials or if these materials are only available for distribution by a for-profit company.

No restrictions.

9. Antibodies

Describe the antibodies used and how they were validated for use in the system under study (i.e. assay and species).

Not antibodies used.

10. Eukaryotic cell lines

a. State the source of each eukaryotic cell line used.

NR8383 cells are an immortalized cell line derived from a lung macrophage (Sprague-Dawley rat). The source is ATCC CRL-2192, Manassas, VA.

b. Describe the method of cell line authentication used.

These cells are used extensively at GSK for drug assays.

c. Report whether the cell lines were tested for mycoplasma contamination.

They have been tested for mycoplasma within GSK.

d. If any of the cell lines used are listed in the database of commonly misidentified cell lines maintained by [ICLAC](#), provide a scientific rationale for their use.

The macrophages used are not listed in the database.

► Animals and human research participants

Policy information about [studies involving animals](#); when reporting animal research, follow the [ARRIVE guidelines](#)

11. Description of research animals

Provide details on animals and/or animal-derived materials used in the study.

mice, strain CD-1, female, typically 6-8 weeks old and were sacrificed by Schedule 1 method.

Policy information about [studies involving human research participants](#)

12. Description of human research participants

Describe the covariate-relevant population characteristics of the human research participants.

No human tissue used.